




Emergent superconducting phases in unconventional p -wave magnets: Topological superconductivity, Bogoliubov Fermi surfaces and superconducting diode effect

Amartya Pal ^{1,2}, Paramita Dutta ^{3,*} and Arijit Saha ^{1,2,†}

¹*Institute of Physics, Sachivalaya Marg, Bhubaneswar-751005, India*

²*Homi Bhabha National Institute, Training School Complex, Anushakti Nagar, Mumbai 400094, India*

³*Theoretical Physics Division, Physical Research Laboratory, Navrangpura, Ahmedabad-380009, India*

The recent discovery of unconventional momentum-dependent magnetic orders has expanded the landscape of magnetism beyond conventional ferromagnetism and antiferromagnetism. Among them, p -wave magnets (p WMs) represent a novel class of odd-parity, non-collinear compensated magnetic order that generates spin-split electronic bands. In this work, our theoretical investigation establishes p WMs as a versatile platform for realizing intriguing superconducting phases including topological superconductivity (TSC), Bogoliubov Fermi surfaces (BFSs), and superconducting diode effect (SDE), within a unified microscopic framework. Employing a minimal model incorporating p -wave magnetic order, exchange coupling, and Zeeman fields, we perform a self-consistent mean-field analysis and uncover a rich phase diagram featuring unconventional finite-momentum Fulde-Ferrell (FF) and Larkin-Ovchinnikov (LO) superconducting phases. Remarkably, we also show that p WMs can undergo a transition to a TSC phase anchoring Majorana flat edge modes, a hallmark of two-dimensional TSCs, even without Rashba spin-orbit coupling and Zeeman field. Upon applying a Zeeman field, gapless FF and LO phases emerge with BFSs characterized by the appearance of finite zero-energy quasiparticle density of states. Furthermore, we demonstrate that SDE arises naturally in the asymmetric FF phase. Our analysis manifests that p WMs serve as a unique and novel platform to host TSC phase, gapless superconducting states, and non-reciprocal transport phenomena.

Introduction

For decades magnetism has been broadly classified into two categories: ferromagnetism and antiferromagnetism, based on their spin ordering. Very recently, this dichotomy has been extended to include momentum-dependent magnetic orders with both even parity altermagnets [1–6] along with odd parity p -wave magnets (p WMs) [7–10]. These unconventional magnets exhibit spin-split electronic bands reminiscent of ferromagnets, while maintaining zero net magnetization, a property of antiferromagnets. The spin-splitting in these systems arises from the absence of combined \mathcal{PT} -symmetry where \mathcal{P} and \mathcal{T} denote the parity and time-reversal symmetry (TRS) operators, respectively. Specifically, p WMs are characterized by $\mathcal{T}\mathbf{t}$ -symmetry where \mathbf{t} denotes the half lattice translation along with broken \mathcal{P} -symmetry [7–9]. Notably, an important feature of the p WMs lies in their non-collinear magnetic order effectively mimics relativistic spin-orbit coupling (SOC) without relying on heavy elements [7–9]. These properties have triggered growing interests and already been explored in some theoretical works [11–16]. Several materials such as CeNiAsO [9], NiI₂ [17], Gd₃(Ru_{1- δ} Rh _{δ})₄Al₁₂ [18] have been proposed as possible candidate materials, while their experimental realization still remains at an early stage [17, 18].

The interplay between magnetism and superconductivity has long been a central theme in condensed matter physics giving rise to a variety of unconventional superconducting phases [19–23], especially, topological superconductivity [24–27] and finite-momentum pairing states [28, 29] etc. While some of the phases have been explored in conventional magnets, and recently in alter-

magnets [30–43], the role of p WMs in realizing such unconventional superconducting orders and their implications are yet to be understood.

Topological superconductivity (TSC) has attracted enormous attention due to its ability to host Majorana zero-energy modes, the charge-neutral quasiparticles obeying non-Abelian statistics and regarded as promising building blocks for fault-tolerant topological quantum computation [24–27]. Existing platforms proposed for realizing Majorana modes, ranging from Rashba nanowires [44–46] and topological insulator surface states [47] to altermagnets [33, 38–40], all rely crucially on the SOC. Given that p WMs intrinsically emulate SOC, they provide a natural platform for studying TSC for which a microscopic picture is essential to identify the ground state.

Another hallmark of the interplay between magnetism and superconductivity is the finite-momentum pairing, in which Cooper pairs condense with a nonzero center-of-mass momentum and leads to periodically modulated superconducting order parameter in the real space [29]. Finite-momentum superconductivity is generally classified into the Fulde-Ferrell (FF) state [48] and the Larkin-Ovchinnikov (LO) state [49]. In the FF phase, all Cooper pairs condense with identical center-of-mass momentum, while in the LO phase, there exists a time-reversal partner with center-of-mass momentum ‘ $-\mathbf{q}$ ’ for every Cooper pair with ‘ \mathbf{q} ’. Remarkably, the attention to the finite-momentum pairing has been renewed recently due to the possibility of the gapless superconducting phases hosting Bogoliubov Fermi surfaces (BFSs) [50] and also for driving superconducting diode effects (SDEs) [51, 52].

In literature, BFSs refer to an unconventional gapless superconducting phase in which the Bogoliubov quasiparticles coexist with Cooper pairs [53–55]. Unlike conventional Bardeen–Cooper–Schrieffer (BCS) superconductors exhibiting a full gap or nodal superconductors with vanishing quasiparticle density of states at zero energy [20], systems with BFSs possess a finite elevated zero-energy density of states [56–60]. The dimension of BFSs is the same as the underlying normal state Fermi surface (FS) which is in sharp contrast to the BCS superconductors [53]. BFSs were theoretically proposed in spin-3/2 systems [53, 54, 61–66], and later shown using BCS [56, 59, 67–69] and d -wave superconductors [55, 57, 60, 70], while they are experimentally observed in Al/InAs heterostructures [71] and in Bi₂Te₃/NbSe₂ hybrid system driven by finite-momentum Cooper pairs [50]. Given the potential to host finite-momentum Cooper pairs in p WMs and the possibility of coexistence of BFS and finite-momentum Cooper pairs, a natural question appears about the generation of BFSs in a gapless phase of p WMs.

Then, in the context of the SDE, another phenomenon driven by finite-momentum Cooper pairs in broken inversion and time-reversal systems, the supercurrent exhibits a non-reciprocal behavior, i.e., $|J_c^+| \neq |J_c^-|$ where, J_c^+ (J_c^-) denotes the critical supercurrent along the forward (reverse) direction [72, 73]. Unlike conventional semiconducting diodes which suffers from the Joule heating, SDE is attractive due to their dissipationless characteristics which are highly promising for device applications. SDE has been experimentally observed in Nb/Ta/V superlattices [74] and later found in other systems such as van der Waals heterostructure [75], small-twist-angle trilayer graphene [76], topological materials [77, 78], and very recently, in altermagnets [79]. It has also been theoretically studied in a wide range of systems including Rashba superconductors [80–83], magnetic adatoms [83, 84], Josephson junctions [85–89], and also in altermagnets [32, 90–92]. While the diode effect in p WM-based Josephson junction is studied very recently [93], microscopic analysis of SDE in bulk p WMs remains unexplored. Given that SDE is known to emerge only in the FF phase in the literature, while it is absent in the LO phase [51, 52, 94], exploring SDE in p WMs presents a natural and compelling direction.

With this wide range of motivation, we address the following intriguing questions: (i) is it possible to find TSC in p WMs without relying on Rashba SOC or any external Zeeman field? (ii) Is there any ground state for the FF or LO phase in p WMs hosting finite-momentum Cooper pairs? (iii) Can finite-momentum pairing induce BFSs in p WMs? (iv) Is it possible to generate SDE and how is it affected by the presence of BFSs? To answer these questions, we consider a p WM characterized by the odd-parity magnetic order and sd -exchange interaction [8] both in the absence and presence of Zeeman

field. First, we analyse the spectral properties of the normal state Hamiltonian in detail to elucidate the role of the exchange coupling and Zeeman splitting. Introducing onsite attractive Hubbard interactions [83, 95], we then perform a fully self-consistent mean-field analysis allowing BCS, FF, and LO pairing channels. We demonstrate that the interplay between the exchange interaction and Zeeman field leads to a rich superconducting phase diagram, as shown in the diagrammatic representation of Fig. 1(a), hosting TSC with Majorana flat edge modes (MFEMs), gapped and gapless FF phases, and a gapless LO phase. We further illustrate that the finite-momentum pairing state drives the system into a gapless phase anchoring BFSs. Finally, we demonstrate the appearance of a tunable SDE in the FF phase, persisting even in the presence of BFSs. Our results establish p WM as a versatile platform for achieving unconventional superconducting phases with possible device application.

Results

Model. We consider a two-dimensional (2D) tight binding Hamiltonian in the momentum-space, $\mathcal{H}_{p\text{WM}}$, that describes a p WM in the normal state with required symmetries, and apply an external Zeeman field B [8]. The total Hamiltonian takes the form:

$$H_N = \sum_{\mathbf{k}} \psi_{\mathbf{k}}^\dagger \mathcal{H}_N(\mathbf{k}) \psi_{\mathbf{k}} = \sum_{\mathbf{k}} \psi_{\mathbf{k}}^\dagger [\mathcal{H}_{p\text{WM}}(\mathbf{k}) + B\sigma_z] \psi_{\mathbf{k}}, \quad (1)$$

where,

$$\begin{aligned} \mathcal{H}_{p\text{WM}}(\mathbf{k}) = & [-2t(\cos k_x + \cos k_y) - \mu]\sigma_0\tau_0 + \alpha \sin k_x \sigma_z \tau_0 \\ & + J_{sd} \sigma_x \tau_z, \end{aligned} \quad (2)$$

and $\psi_{\mathbf{k}} = \{c_{\mathbf{k}A\uparrow}, c_{\mathbf{k}B\uparrow}, c_{\mathbf{k}A\downarrow}, c_{\mathbf{k}B\downarrow}\}^T$ with $c_{\mathbf{k}\gamma,s}$ ($c_{\mathbf{k}\gamma,s}^\dagger$) representing the annihilation (creation) operator for an electron with momentum $\mathbf{k} = \{k_x, k_y\}$ and spin $s = \{\uparrow, \downarrow\}$ in the orbital $\gamma = \{A, B\}$. The Pauli matrices σ and τ act on the spin and orbital degrees of freedom, respectively. The model parameters t and μ represent the nearest-neighbour hopping amplitudes and the chemical potential, respectively. Importantly, α and J_{sd} parametrize the p -wave magnetic exchange orders which originates from the exchange interaction between the itinerant electrons and the localized non-collinear magnetic moments [8, 11]. Specifically, α corresponds to the spin-dependent hopping amplitude and J_{sd} denotes the isotropic sd -coupling between itinerant electrons and localized moments, featuring partially spin-polarized bands. As discussed previously, $\mathcal{H}_{p\text{WM}}(\mathbf{k})$ preserves the TRS i.e., $\mathcal{T}\mathcal{H}_{p\text{WM}}(-\mathbf{k})\mathcal{T}^{-1} = \mathcal{H}_{p\text{WM}}(\mathbf{k})$ where $\mathcal{T} = i\sigma_y\tau_x\mathcal{K}$ with \mathcal{K} being the complex conjugation operator. Needless to say, the TRS is broken when the magnetic field B is switched on. Here, the external magnetic field only couples with the spin degrees of freedom neglecting the orbital effects [32]. We consider $\mu = -2t$ unless otherwise specified and set $t = 1$ (in units of energy).

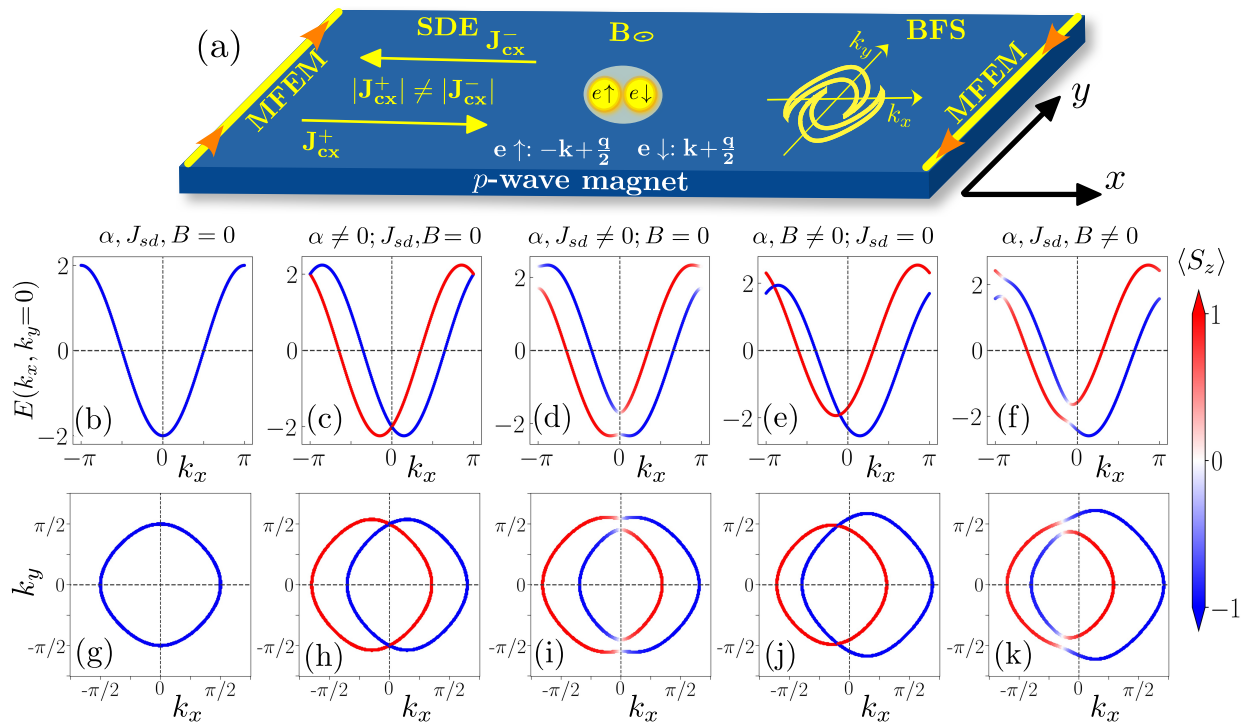


FIG. 1. **Illustration of the unconventional superconducting phases and the normal state spectral properties.** (a) Schematic illustration for possible phases in p WM in the presence of an external Zeeman field B , along with the MFEMs at the boundary. In panels, (b)-(f) [(g)-(k)] bulk energy-spectrum [Fermi surfaces] along with spin-polarization $\langle S_z \rangle$ (in units of $\hbar/2$) have been demonstrated. Other model parameter values are chosen as (b),(g) $(\alpha, J_{sd}, B) = (0, 0, 0)$, (c),(h) $(\alpha, J_{sd}, B) = (t, 0, 0)$, (d),(i) $(\alpha, J_{sd}, B) = (t, 0.3t, 0)$, (e),(j) $(\alpha, J_{sd}, B) = (t, 0, 0.3t)$, (f),(k) $(\alpha, J_{sd}, B) = (t, 0.3t, 0.3t)$ with $t = 1$ and $\mu = -2t$.

Focussing on the spectral features of the normal state to understand the role of each model parameters and the magnetic field, we first compute the bulk spectrum and the FS by diagonalizing $\mathcal{H}_N(k)$. Then, we compute the expectation value of the spin polarization along the z -direction i.e., $\langle S_z \rangle_{\mathbf{k}} = \frac{\hbar}{2} \langle \sigma_z \rangle_{\mathbf{k}} = \frac{\hbar}{2} \langle u_{\mathbf{k}} | \sigma_z | u_{\mathbf{k}} \rangle$, where $|u_{\mathbf{k}}\rangle$ is the eigenvector of the Hamiltonian $\mathcal{H}_N(\mathbf{k})$ with eigenvalue $E(\mathbf{k})$. We depict the bulk spectrum $E(k_x, k_y = 0)$ as a function of k_x in Figs. 1(b)-(f) and the FS in the $k_x - k_y$ plane in Figs. 1(g)-(k) for various choices of model parameters. We also display the spin-polarization, $\langle S_z \rangle_{\mathbf{k}}$ (in units of $\hbar/2$) on top of bulk spectrum and FS in each plot.

In Figs. 1(b) and (g), when $\alpha, J_{sd}, B = 0$, we observe the bulk bands to be four-fold degenerate along with the degenerate FS. When $\alpha \neq 0$ (keeping $J_{sd}, B = 0$), the bulk bands as well as the FS split along k_x -direction lifting the four-fold degeneracy except at $k_x = 0, \pi$ (see Figs. 1(c) and (h)). Note that, the FS remains spin-polarized as $\mathcal{H}_N(\mathbf{k})$ commutes with σ_z , i.e., $[\mathcal{H}_N(\mathbf{k}), \sigma_z] = 0$. Now, if we consider both $\alpha, J_{sd} \neq 0$ (still $B = 0$), the four-fold degeneracy at $k_x = 0, \pi$ for the band as well as FS is lifted as shown in Figs. 1(d) and (i). The FS becomes partially spin-polarized in this parameter space since $[\mathcal{H}_N(\mathbf{k}), \sigma_z] \neq 0$ (see Fig. 1(i)). How-

ever, the TRS is still respected in the system which is reflected in the presence of Kramer's pairs maintaining $E(\mathbf{k}, s) = E(-\mathbf{k}, -s)$ where the spin $s = \langle S_z \rangle_{\mathbf{k}}$.

So far, the magnetic field is switched off in our consideration. In the presence of a magnetic field, when $\alpha \neq 0$ and $J_{sd} = 0$, the system breaks TRS, lifting the Kramer's degeneracy i.e., $E(\mathbf{k}, s) \neq E(-\mathbf{k}, -s)$ as visible in the energy spectrum of Fig. 1(e), whereas the corresponding FS becomes fully spin-polarized (see Fig. 1(j)) as $[\mathcal{H}_N(\mathbf{k}), \sigma_z] = 0$. Finally, when we turn on all the three components i.e., $\alpha, J_{sd}, B \neq 0$, the bulk bands as well as the FS (see Figs. 1(f) and (k)) are partially spin-polarized. Notably, the bands and FS become asymmetric with respect to k_x indicating the possibility of finite-momentum pairing both in the absence and presence of J_{sd} as long as $\alpha, B \neq 0$. For any state with momentum and spin $\{\mathbf{k}, s\}$, the partner state with $\{-\mathbf{k}, -s\}$ is not available, restricting the formation of conventional BCS type pairing, which we discuss in the upcoming sections in more detail.

Mean-field analysis. In order to investigate the possible superconducting orders in the normal state Hamiltonian of p WMs, we consider an attractive onsite electron-

electron interaction of the form,

$$H_U = -U \sum_{\mathbf{r}, \gamma = \{A, B\}} n_{\mathbf{r}\gamma\uparrow} n_{\mathbf{r}\gamma\downarrow}, \quad (3)$$

where, $n_{\mathbf{r}\gamma s} = c_{\mathbf{r}\gamma, s}^\dagger c_{\mathbf{r}\gamma s}$ with $c_{\mathbf{r}\gamma, s}^\dagger$ being the electron creation operator at position \mathbf{r} in the orbital γ with spin s . Here, $U (> 0)$ is the strength of attractive interaction. Origin of such electron-electron correlation can be intrinsic to the system [20, 96] or can be induced via the proximity effect [22, 97]. We can rewrite the interaction term in momentum space as,

$$H_U = -\frac{U}{N} \sum_{\mathbf{k}_1, \mathbf{k}_2, \mathbf{k}_3, \gamma} c_{\mathbf{k}_1 + \mathbf{k}_3 \gamma \uparrow}^\dagger c_{\mathbf{k}_2 - \mathbf{k}_3 \gamma \downarrow}^\dagger c_{\mathbf{k}_2 \gamma \downarrow} c_{\mathbf{k}_1 \gamma \uparrow}, \quad (4)$$

where, N is the grid size of the Brillouin zone. Then, we perform a mean-field decomposition into the conventional BCS and also into the unconventional finite-momentum FF and LO pairing channels which is of our primary interest. For the finite-momentum pairing channel, we consider $\mathbf{k}_2 = -\mathbf{k}_1 + \mathbf{q}$ with $\mathbf{q} = \{q_x, q_y\}$ being the center-of-mass momentum of the Cooper pair. The order parameters corresponding to these three pairing channels are defined as [29]:

$$\Delta^{\text{BCS}} = -\frac{U}{N} \sum_{\mathbf{k}} \langle c_{-\mathbf{k}\gamma\downarrow} c_{\mathbf{k}\gamma\uparrow} \rangle, \quad (5)$$

$$\Delta_{\mathbf{q}}^{\text{FF}} = -\frac{U}{N} \sum_{\mathbf{k}} \langle c_{-\mathbf{k} + \frac{\mathbf{q}}{2} \gamma \downarrow} c_{\mathbf{k} + \frac{\mathbf{q}}{2} \gamma \uparrow} \rangle, \quad (6)$$

$$\Delta_{\mathbf{q}}^{\text{LO}} = -\frac{U}{2N} \sum_{\mathbf{k}} [\langle c_{-\mathbf{k} + \frac{\mathbf{q}}{2} \gamma \downarrow} c_{\mathbf{k} + \frac{\mathbf{q}}{2} \gamma \uparrow} \rangle + \langle c_{-\mathbf{k} - \frac{\mathbf{q}}{2} \gamma \downarrow} c_{\mathbf{k} - \frac{\mathbf{q}}{2} \gamma \uparrow} \rangle]. \quad (7)$$

Interestingly, the order parameter for the FF channel $\Delta_{\mathbf{q}}^{\text{FF}}$ appears to be the most general one. It takes into account both the BCS and LO pairing channels, explicitly, $\Delta^{\text{BCS}} = \Delta_{\mathbf{q}=0}^{\text{FF}}$ and $\Delta_{\mathbf{q}}^{\text{LO}} = (\Delta_{\mathbf{q}}^{\text{FF}} + \Delta_{-\mathbf{q}}^{\text{FF}})/2$. Thus, we only consider $\Delta_{\mathbf{q}}^{\text{FF}}$ throughout the rest of the discussions to characterize the superconducting ground state. Also, throughout the rest of the manuscript, we drop the label γ assuming equal magnitude of intra-orbital pairing amplitude.

The Bogoliubov-de Gennes (BdG) Hamiltonian after the mean-field decomposition becomes

$$H_{\text{BdG}} = \frac{1}{2} \sum_{\mathbf{k}} \Psi_{\mathbf{k}\mathbf{q}}^\dagger \mathcal{H}_{\text{BdG}}(\mathbf{k}, \mathbf{q}) \Psi_{\mathbf{k}\mathbf{q}} + \frac{2N}{U} |\Delta_{\mathbf{q}}^{\text{FF}}|^2 + \text{const.} \quad (8)$$

where, $\Psi_{\mathbf{k}\mathbf{q}} = (c_{\mathbf{k} + \frac{\mathbf{q}}{2} A \uparrow}, c_{\mathbf{k} + \frac{\mathbf{q}}{2} B \uparrow}, c_{\mathbf{k} + \frac{\mathbf{q}}{2} A \downarrow}, c_{\mathbf{k} + \frac{\mathbf{q}}{2} B \downarrow}, c_{-\mathbf{k} + \frac{\mathbf{q}}{2} A \uparrow}^\dagger, c_{-\mathbf{k} + \frac{\mathbf{q}}{2} B \uparrow}^\dagger, c_{-\mathbf{k} + \frac{\mathbf{q}}{2} A \downarrow}^\dagger, c_{-\mathbf{k} + \frac{\mathbf{q}}{2} B \downarrow}^\dagger)^T$ is the Nambu spinor and

$$\mathcal{H}_{\text{BdG}}(\mathbf{k}, \mathbf{q}) = \begin{bmatrix} \mathcal{H}_N(\mathbf{k} + \frac{\mathbf{q}}{2}) & -i\sigma_y \Delta_{\mathbf{q}}^{\text{FF}} \\ i\sigma_y \Delta_{\mathbf{q}}^{\text{FF}} & -\mathcal{H}_N^T(-\mathbf{k} + \frac{\mathbf{q}}{2}) \end{bmatrix} \quad (9)$$

with $\mathcal{H}_N(\mathbf{k} + \frac{\mathbf{q}}{2})$ is the normal state Hamiltonian (see Eq. (1)).

We now define the condensation energy density, $\Omega(\mathbf{q}, \Delta_{\mathbf{q}}^{\text{FF}})$, at the superconducting ground state as [29], $\Omega(\mathbf{q}, \Delta_{\mathbf{q}}^{\text{FF}}) = \mathcal{F}(\mathbf{q}, \Delta_{\mathbf{q}}^{\text{FF}}) - \mathcal{F}(\mathbf{q}, 0)$, where $\mathcal{F}(\mathbf{q}, \Delta_{\mathbf{q}}^{\text{FF}})$ and $\mathcal{F}(\mathbf{q}, 0)$ represent the free energy density at the superconducting and normal state of the system, respectively. At near zero temperature, the free energy density is computed using the relation [98]: $\mathcal{F}(\mathbf{q}, \Delta_{\mathbf{q}}^{\text{FF}}) = \frac{1}{N} \sum_{\mathbf{k}, \mathcal{E}(\mathbf{k}, \mathbf{q}) < 0} \mathcal{E}(\mathbf{k}, \mathbf{q}) + \frac{2N}{U} |\Delta_{\mathbf{q}}^{\text{FF}}|^2$

where $\mathcal{E}(\mathbf{k}, \mathbf{q})$ is the energy eigenvalue of the BdG Hamiltonian (Eq. (S1)). The critical values of $\Delta_{\mathbf{q}}^{\text{FF}}$, q_x , and q_y denoted by (Δ^c, q_x^c, q_y^c) that minimize the condensation energy are computed by self-consistently capturing the energetically most favored state. In our numerical calculation, we set $U/2t = 1.5$, $\mu/2t = -1$, $\alpha/t = 1$ (unless otherwise specified) and consider a 500×500 ($N = 25 \times 10^4$) momentum-space grid size. Changing these numerical values do not affect our main results qualitatively, unless the Hubbard strength is large for which the mean-field treatment will no longer remain valid.

By investigating the superconducting ground state throughout the parameter space, we obtain a rich phase diagram demonstrated in Fig. 2 and provide a comprehensive analysis of all the phases. For $J_{sd} = B = 0$, the superconducting ground state is given by $(\Delta^c, q_x^c, q_y^c) = (0.43t, 0, 0)$ which corresponds to the conventional BCS ground state hosting zero-momentum Cooper pairs (s -wave). We define $\Delta^c|_{J_{sd}, B=0} \equiv \Delta_0$ and scale Δ^c by Δ_0 . We then analyse self-consistently computed $\Delta^c/\Delta_0, q_x^c$, and q_y^c in the plane of J_{sd} and B as shown in Figs. 2(a), (b), and (c), respectively. We identify various superconducting phases in Fig. 2(a) that includes conventional BCS, gapped FF, gapless FF, and gapless LO phases.

When $J_{sd} = 0$, then if we only vary the magnetic field B , then the system evolves from a conventional s -wave to a state with finite-momentum pairing (see Fig. 2(a)) but only along y -direction i.e., $q_x^c = 0$ and $q_y^c \neq 0$, as confirmed from Figs. 2(b) and (c). The variation of $\Omega(\mathbf{q})$ in this phase (see inset of Fig. 2(c)) indicates the existence of two degenerate ground states at $(q_x, q_y) = (0, \pm q_y^c)$, thus confirming it to be the finite-momentum pairing state in the LO channel. Interestingly, the transition from the BCS to the LO state takes place at a critical value of the Zeeman field $B^c = 0.7\Delta_0 \simeq \Delta_0/\sqrt{2}$ which corresponds to the Chandrasekhar-Clogston limit or Pauli limit [99, 100]. This limit refers to the critical strength of the external Zeeman field above which the conventional BCS state transforms to a normal metallic state. However, a finite-momentum pairing state can be stable even above this limit [29], as reflected in the phase diagram.

Then, when $J_{sd} \neq 0$, we find the LO state is stable over a certain finite value of J_{sd} above which (for any finite

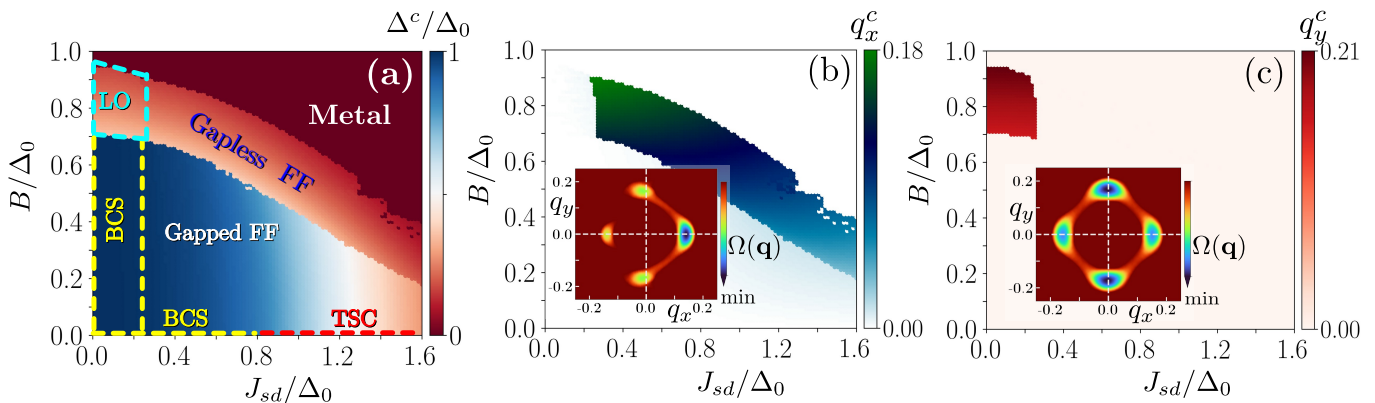


FIG. 2. **Phase diagram for the superconducting ground state:** Behavior of the (a) superconducting order parameter Δ^c/Δ_0 , (b) q_x^c and (c) q_y^c are depicted across the parameter space spanned by J_{sd} and B . In panel (a), we highlight the unconventional superconducting phases, TSC along with gapped FF, gapless FF, and LO pairing states. Inset of (b) and (c) display the condensation energy density, $\Omega(\mathbf{q}, \Delta_{\mathbf{q}}^{\text{FF}})$, in the q_x - q_y plane, corresponding to the gapless FF [$(J_{sd}, B) = (0.5, 0.7)\Delta_0$] and gapless LO [$(J_{sd}, B) = (0, 0.75)\Delta_0$] state, respectively.

strength of B) the FF pairing state becomes energetically more favorable with a finite Cooper pair momentum along x -direction ($q_x^c \neq 0$) while $q_y^c = 0$ (see inset of Fig. 2(b)). Since, there is only one ground state, we confirm this to be the FF state. As we increase the strength of B , the system remains in the FF pairing state however the spectral gap of the BdG Hamiltonian vanishes. This transition from the gapped to gapless FF pairing state is associated with a discontinuous change in (Δ^c, q_x^c) (see supplementary materials (SM) for details). Thus, we successfully uncover the possible finite-momentum pairing states in p WMs in the presence of an external Zeeman field.

With the understanding of the finite-momentum pairing states, we next discuss the implications corresponding to these states. Interestingly, the system undergoes a transition to the TSC phase at $J_{sd}^c = 0.8\Delta_0$ in the absence of the external Zeeman field as illustrated in Fig. 2(a) which we discuss in detail as follows.

Topological superconductivity:

In order to establish the emergence of topological phase in our system, we systematically analyse the eigenvalues and eigenvectors of $\mathcal{H}_{\text{BdG}}(\mathbf{k}, \mathbf{q})$ within the bulk as well as at the boundary. When $B = 0$, we can rewrite $\mathcal{H}_{\text{BdG}}(\mathbf{k}, \mathbf{q})$ of Eq. (S1) in the BCS s -wave pairing channel in a compact form as,

$$\mathcal{H}_{\text{BdG}}^{\text{BCS}}(\mathbf{k}) = \xi(\mathbf{k})\pi_z + \alpha(\mathbf{k})\sigma_z + J_{sd}\pi_z\sigma_x\tau_z + \Delta^c\pi_y\sigma_y, \quad (10)$$

where, $\xi(\mathbf{k}) = [-2t(\cos k_x + \cos k_y) - \mu]$, $\alpha(\mathbf{k}) = \alpha \sin k_x$, and π denotes the Pauli matrices acting on the particle-hole degree of freedom. Note that, Δ^c is obtained self-consistently by minimizing the condensation energy density; thus it depends on J_{sd} .

In Fig. 3(a), we depict the bulk energy spectrum $\mathcal{E}(\mathbf{k})$ by diagonalizing $\mathcal{H}_{\text{BdG}}^{\text{BCS}}(\mathbf{k})$ for $J_{sd}(=1.4\Delta_0) > J_{sd}^c$. One can observe the appearance of four isolated nodal points

where the valence and conduction bands touch each other resulting in a gapless superconducting state. The presence of a topological phase is manifested in the bulk-boundary correspondence. To examine this, we next consider a ribbon geometry where the system is periodic along y -direction and finite only along x -direction with the length $L_x = 100a$ ($a = 1$) being the lattice spacing. The Hamiltonian for this ribbon geometry is obtained by performing an inverse Fourier transformation along x -direction (see methods section for details) and the corresponding band structure is depicted in Fig. 3(b) as a function of k_y showcasing the emergence of flat Majorana zero-energy modes connecting the bulk nodal points i.e., weak TSC phase.

To further investigate the localization property of these flat zero-energy modes, we consider the system under the open-boundary condition in both directions i.e., a rectangular geometry being finite size along both x - and y -direction with $(L_x, L_y) = (60a, 100a)$. Then, we again diagonalize the Hamiltonian for this geometry and show the behavior of the eigenvalues \mathcal{E}_n as a function of state index n in the inset of Fig. 3(c). Additionally, we compute the site-resolved local density of states (LDOS) at energy \mathcal{E} using the expression: $\text{LDOS}(\mathbf{r}, \mathcal{E}) = \sum_n \delta(\mathcal{E} - \mathcal{E}_n) |\langle \mathbf{r} | u_n(\mathbf{r}) \rangle|^2$, where $|u_n(\mathbf{r})\rangle$ is the eigenvector having eigenvalue \mathcal{E}_n and $\delta(x)$ is the Dirac-delta function. We illustrate the LDOS (at $\mathcal{E} = 0$) in Fig. 3(c) as a function of real-space lattice coordinates. From the LDOS profile, it is evident that LDOS is finite and highest in magnitude at the two edges along y -direction located at $x = 0$ and $x = L_x$, while it vanishes as we proceed towards the bulk of the system. The energy eigenvalues together with the LDOS clearly establish that the Majorana flat zero-energy modes are localized at the boundary of the system.

With these findings of the gapless boundary along with

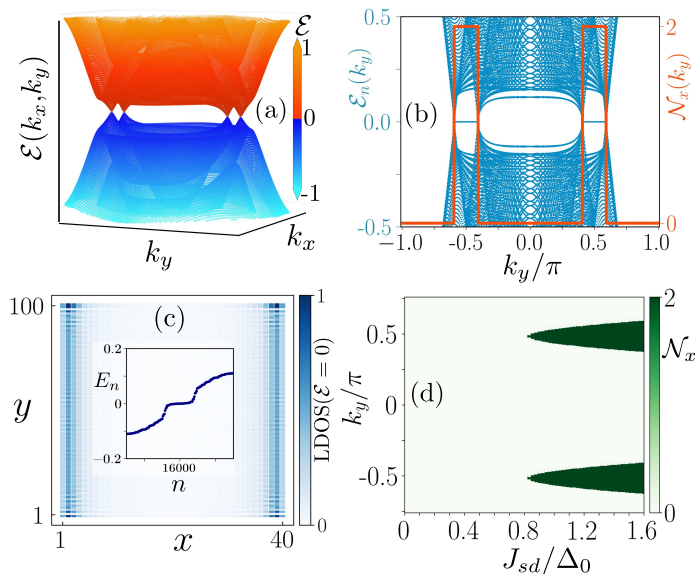


FIG. 3. **Emergence of topological superconductivity:** (a) Bulk energy spectrum is shown in the TSC phase in the $k_x - k_y$ plane exhibiting four isolated nodal points. (b) Eigenvalue spectrum (left axis) and winding number (right axis) are shown as a function of k_y considering finite size along x -direction. (c) LDOS profile at zero energy is shown in the co-ordinate space for the rectangular geometry. Inset displays the variation of energy-eigenvalues E_n as a function of state index, n , manifesting the flat zero energy modes. (d) Variation of winding number, \mathcal{N}_x , is shown in the $J_{sd} - k_y$ plane. In panels (a)-(c), we choose $(J_{sd}, B) = (1.4\Delta_0, 0)$ corresponding to the TSC phase of Fig. 2(a) and set $B = 0$ in panel (d).

the zero-energy boundary modes, we further investigate the topological origin of these zero-energy flat edge modes by calculating a topological invariant. As mentioned earlier, in the absence of any external Zeeman field, the system retains TRS. Additionally, the charge-conjugation symmetry $\mathcal{C} = \pi_x \mathcal{K}$ and the chiral symmetry $\mathcal{S} = \pi_x \sigma_y \tau_x$ are also preserved i.e., $\mathcal{C}^{-1} \mathcal{H}_{\text{BdG}}^{\text{BCS}}(\mathbf{k}) \mathcal{C} = -\mathcal{H}_{\text{BdG}}^{\text{BCS}}(-\mathbf{k})$ and $\mathcal{S}^{-1} \mathcal{H}_{\text{BdG}}^{\text{BCS}}(\mathbf{k}) \mathcal{S} = -\mathcal{H}_{\text{BdG}}^{\text{BCS}}(\mathbf{k})$. Thus, our system in the BCS channel belongs to the BDI topological class with a \mathbb{Z} invariant in one-dimension [101]. Topological characterization of the flat edge modes in 2D TSCs can be performed by computing the winding number \mathcal{N}_x as a function of k_y as [101–104]:

$$\mathcal{N}_x(k_y) = \frac{i}{2\pi} \int_{\text{BZ}} dk_x \text{Tr} [q^{-1}(\mathbf{k}) \partial_{k_x} q(\mathbf{k})], \quad (11)$$

where, $q(\mathbf{k})$ is obtained by recasting $\mathcal{H}_{\text{BdG}}^{\text{BCS}}(\mathbf{k})$ into an anti-diagonal form by utilizing the presence of chiral symmetry in the system. Note that, $q(\mathbf{k})$ is constructed using the self-consistently computed values of Δ^c (see methods section). We depict the behavior of winding number \mathcal{N}_x as a function of k_y in Fig. 3(d) and find a perfect one-to-one correspondence between the Majorana flat-edge modes and non-zero \mathcal{N}_x value, explicitly, $\mathcal{N}_x = 2$. This

establishes the emergence of MFEMs as a manifestation of the TSC phase in p WMs.

Before we conclude this discussion, we illustrate the variation of \mathcal{N}_x in the $J_{sd} - k_y$ plane to identify the parameter regime corresponding to the TSC phase as demonstrated in Fig. 3(d). It clearly shows the onset of TSC phase at $J_{sd} = 0.8\Delta_0$. Our findings are also consistent with the time-reversal symmetric 2D TSC having $(p_x + p_y)$ -pairing symmetry and MFEMs proposed in the literature [105]. Therefore, we successfully establish the emergence of weak TSC phase in the BCS pairing channel hosting MFEMs without employing any external Zeeman field. Importantly, we do not need any Rashba SOC to obtain this TSC in contrast to the majority of the proposal reported in literature on MFEMs [106, 107].

Bogoliubov Fermi surfaces: We now examine the emergence of BFSs as a direct consequence of finite momentum superconductivity. Since BFSs appear in the gapless superconducting phase, we investigate the presence of BFSs in the gapless LO and also in the gapless FF state. We choose two sets of $(J_{sd}/\Delta_0, B/\Delta_0)$ from the phase diagram of Fig. 2(a): one from the gapless LO state with $(J_{sd}/\Delta_0, B/\Delta_0) = (0, 0.72)$, and the other from the gapless FF state with $(J_{sd}/\Delta_0, B/\Delta_0) = (0.9, 0.6)$. We also examine the characteristics of FSs corresponding to these parameter values in Fig. 4(a) (LO state) and Fig. 4(b) (FF state), and identify them as BFSs based on the following points. First, the dimensions of these FSs are the same as the underlying normal state FSs, which is one of the defining property of BFSs [53, 55]. Secondly, there exists a substantial population of Bogoliubov quasiparticles in addition to Cooper pairs and are primarily characterized by the finite density of states around zero energy [55]. To establish this, we compute the single particle density of states using $\text{DOS}(E) = \sum_{\mathbf{k}} \delta(E - \mathcal{E}(\mathbf{k}))$, where $\mathcal{E}(\mathbf{k})$ are the energy-eigenvalues of the mean-field BdG Hamiltonian $\mathcal{H}_{\text{BdG}}(\mathbf{k}, \mathbf{q})$ and show it as a function of E/Δ_0 in Fig. 4(c) for both the LO and FF states. To emphasize, the DOS is computed with the self-consistently obtained values of (Δ^c, q_x^c, q_y^c) . Importantly, we find an elevated DOS around the zero energy, indicating the presence of the Bogoliubov quasiparticles as zero-energy excitations. Note that, the elevated DOS is larger in magnitude in case of FF state due to the additional satellite structures of BFSs (see Fig. 4(b)). Additionally, we also observe the presence of superconducting coherence peaks at $E/\Delta_0 \sim 0.33$ in the LO state and at $E/\Delta_0 \sim 0.2$ for the FF state, which also support the self-consistently obtained values of Δ^c in both the LO and FF state. Therefore, our analysis confirms the appearance of BFSs in the gapless LO and FF states driven by the finite-momentum Cooper pairs.

Now, to demonstrate the appearance of BFSs throughout the gapless LO and FF phases, we compute the DOS ($E = 0$) by scanning the model parameters (J_{sd}, B) with

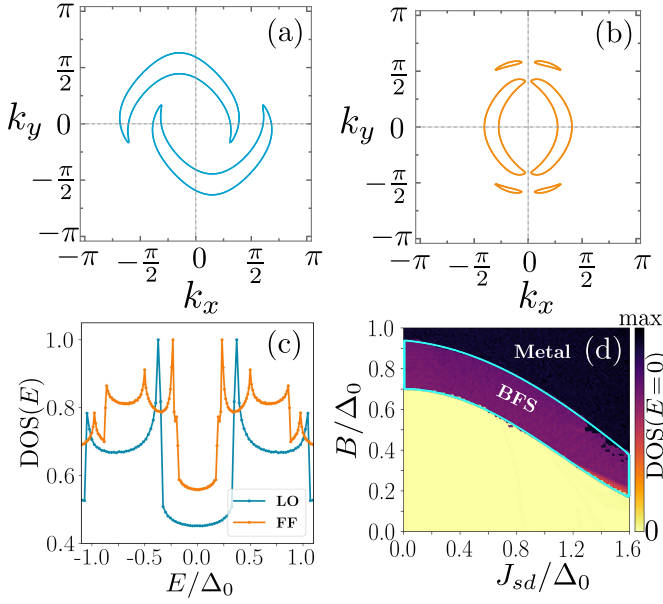


FIG. 4. **Emergence of BFs driven by finite-momentum Cooper pairs:** Demonstration of the appearance of BFs in the $k_x - k_y$ plane corresponding to the gapless (a) LO and (b) FF phase. (c) Normalized single-particle density of states is shown as a function of E/Δ_0 in the gapless finite-momentum superconductivity channels. (d) Phase diagram of the zero energy density of states is displayed in the $J_{sd} - B$ plane, highlighting the presence of BFs in the gapless superconducting phases.

the self-consistently obtained values of (Δ^c, q_x^c, q_y^c) and illustrate in Fig. 4(d). We observe that the nonzero finite DOS (at $E = 0$) appears in the gapless LO, gapless FF, and in the normal state. The nonzero DOS in the normal state appears due to the metallic nature of the underlying normal state system, whereas the finite elevated DOS ($E = 0$) in the LO and FF state represent the emergence of BFs. Thus, we establish a novel pathway for hosting BFs driven by the finite-momentum superconductivity.

Superconducting diode effect: Finally, we focus on another important manifestation of the finite-momentum superconductivity in p WMs: the appearance of SDE [51, 72]. To achieve this, we compute the supercurrent density, $\mathbf{J}(\mathbf{q})$, defined as [52],

$$J_i(\mathbf{q}) = 2e \frac{\partial \Omega(q_x, q_y, \Delta_{\mathbf{q}}^0)}{\partial q_i}, \quad i = (x, y), \quad (12)$$

where, e is the charge of the electron, $\Omega(q_x, q_y, \Delta_{\mathbf{q}}^0)$ is the condensation energy density for a given value of $\mathbf{q} = (q_x, q_y)$ and $\Delta_{\mathbf{q}}^0$ is the superconducting pairing amplitude obtained self-consistently after minimizing $\Omega(q_x, q_y, \Delta_{\mathbf{q}}^{\text{FF}})$ with respect to $\Delta_{\mathbf{q}}^{\text{FF}}$ i.e., $\Omega(\mathbf{q}, \Delta_{\mathbf{q}}^0) \equiv \min_{\Delta_{\mathbf{q}}^{\text{FF}}} \Omega(\mathbf{q}, \Delta_{\mathbf{q}}^{\text{FF}})$. Thus, for the actual superconducting ground state, $\mathbf{q}^c = (q_x^c, q_y^c)$, the supercurrent density $\mathbf{J}(\mathbf{q}^c) = 0$ by definition.

To quantify the SDE, we define diode efficiency factor,

defined in terms of the critical supercurrent density as,

$$\eta_i = \frac{|J_i^{c+} - J_i^{c-}|}{J_i^{c+} + J_i^{c-}}, \quad i = x, y \quad (13)$$

where, J_i^{c+} (J_i^{c-}) refers to the critical supercurrent densities along the positive (negative) i -direction, i.e., $J_i^{c+} \equiv \max_{\mathbf{q}} J_i(\mathbf{q})$ and $J_i^{c-} \equiv |\min_{\mathbf{q}} J_i(\mathbf{q})|$. For the upcoming discussions on SDE, we follow the convention that the positive (negative) values of $J_i(\mathbf{q})$ represent the flow of supercurrent along the positive (negative) i ($i \in \{x, y\}$)-direction. We also emphasize that the SDE is observed only in the FF phase, not in the LO pairing state. This is because in the FF state, the Cooper pairs condense into a unique finite center-of-mass momentum $\mathbf{q}^c = \{q_x^c, q_y^c\}$ without having any TRS partner momentum at $-\mathbf{q}^c$. For our system, in the FF state, the condensation energy density, $\Omega(q_x, q_y, \Delta_{\mathbf{q}}^0)$ is symmetric with respect to q_y i.e., $\Omega(q_x, q_y, \Delta_{\mathbf{q}}^0) = \Omega(q_x, -q_y, \Delta_{\mathbf{q}}^0)$, however asymmetric with respect to q_x i.e., $\Omega(q_x, q_y, \Delta_{\mathbf{q}}^0) \neq \Omega(-q_x, q_y, \Delta_{\mathbf{q}}^0)$. Consequently, the critical current density along x -direction becomes non-reciprocal, i.e., $J_x^{c+} \neq J_x^{c-}$ leading to nonzero values of only η_x . In contrast, the critical current density along y -direction is completely reciprocal: $J_y^{c+} = J_y^{c-}$. This can be explicitly argued in the following way. If the supercurrent density along y -direction attains its maximum value when $\mathbf{q} = (q_x^m, q_y^m)$ i.e., $J_y(q_x^m, q_y^m) = J_y^{c+}$, then there exists a point with $\mathbf{q} = (q_x^m, -q_y^m)$ where $J_y(q_x^m, -q_y^m) = 2e \frac{\partial \Omega(q_x^m, -q_y^m, \Delta_{\mathbf{q}}^0)}{\partial (-q_y^m)} = -2e \frac{\partial \Omega(q_x^m, q_y^m, \Delta_{\mathbf{q}}^0)}{\partial (q_y^m)} = -J_y^{c+}$. Thus, the critical supercurrent density along y -direction is perfectly reciprocal. Similarly, it can be shown that in the LO pairing state, the behavior of the critical supercurrent density $\mathbf{J}(\mathbf{q})$ is reciprocal as $\Omega(q_x, q_y, \Delta_{\mathbf{q}}^0) = \Omega(-q_x, q_y, \Delta_{\mathbf{q}}^0) = \Omega(q_x, -q_y, \Delta_{\mathbf{q}}^0)$.

We now compute the supercurrent density $\mathbf{J}(\mathbf{q})$ numerically using Newton's central difference method and depict the behavior of both $J_x(\mathbf{q})$ and $J_y(\mathbf{q})$ in Fig. 5(a) and (b), respectively, corresponding to the gapless FF phase with $(J_{sd}/\Delta_0, B/\Delta_0) = (0.5, 0.7)$. We observe that $J_x^{c+} \neq J_x^{c-}$ but $J_y^{c+} = J_y^{c-}$, as discussed in the previous paragraph, thus, we focus on only η_x ($\equiv \eta$). In Fig. 5(c), we showcase the variation of η as a function of the Zeeman field considering $\mu/t = -2, -2.1, -2.2$ with $J_{sd} = 0.5t$. We find the maximum diode efficiency with $\eta = 27\%$ for $\mu = -2.2t$. We refer to the SM for the variation of (q_x^c, q_y^c, Δ^c) as well as the superconducting bulk gap.

We further study the variation of η for different choices of J_{sd} maintaining fixed μ and show the behavior in Fig. 5(d). In this parameter space, we find the maximum value of $\eta \sim 33\%$. Note that, in both cases, η initially increases with the increase in B upto a critical value of B , after which η decreases with increasing in B . At this critical value of B , the system enters into the gapless FF phase from the gapped FF phase (see SM for the details

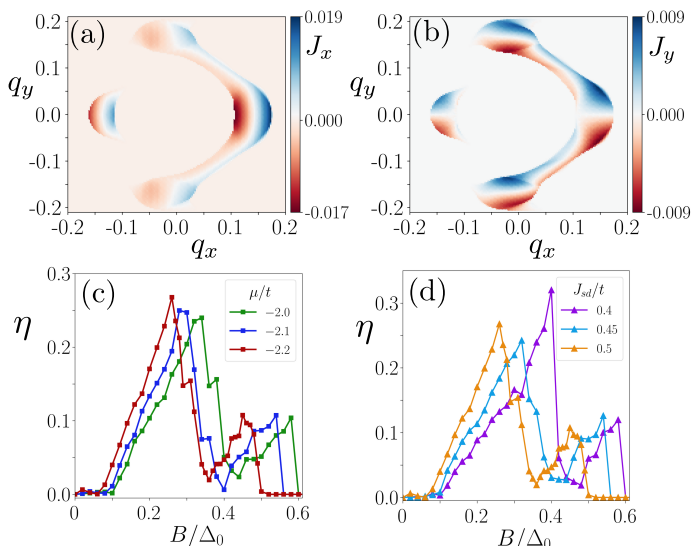


FIG. 5. **Manifestation of SDE in the FF pairing channel:** In panels (a) and (b), the variation of supercurrent $J_x(\mathbf{q})$ and $J_y(\mathbf{q})$, respectively, are shown in the $q_x - q_y$ plane corresponding to the FF pairing state with $(J_{sd}/\Delta_0, B/\Delta_0) = (0.5, 0.7)$. Panels (c) and (d) display the Diode efficiency factor, η , as a function of the external Zeeman field, B for various choices of μ and J_{sd} , respectively. We choose the other model parameters as $(J_{sd}, \alpha) = (0.5t, t)$ in panel (c) and $(\mu, \alpha) = (-2.2t, t)$ in panel (d).

of the bulk BdG gap). This gapless FF phase hosts BFSs as zero-energy excitation, comprised of both the Bogoliubov quasiparticles and Cooper pairs. Thus, density of Cooper pairs is diluted in the gapless state compared to the gapped FF state. This causes the suppression of η in the gapless FF state. Interestingly, we also find that within the gapless FF state, η increases further with increasing B before vanishes where the superconductivity is completely destroyed. Therefore, from our analysis, we establish the manifestation of finite-momentum superconductivity in the FF state as a mechanism for SDE. Thus, p WMs can be a potential candidate for application in realizing dissipationless superconducting devices.

Discussion

To summarize, we have demonstrated that p WMs provide a promising platform for realizing a rich variety of unconventional superconducting phases. These include TSC along with finite-momentum pairing in both FF and LO pairing states. The inherent momentum-dependent spin splitting combined with the intrinsic exchange interaction drives the system into the emergence of topological phases without requiring any external Zeeman field or Rashba spin-orbit coupling, thereby opening routes toward scalable device applications. On the other hand, in the presence of a Zeeman field, the Cooper pairs acquire finite center-of-mass momentum driving the system into a gapless phase hosting BFSs as a zero-energy excitations with potential of applications in quantum de-

vices. Additionally, the emergence of the SDE has also been established in the FF phase, drawing attention as an energy-efficient superconducting device component. On a final note, the superconductivity in our model has been treated within a self-consistent mean-field BdG formalism, ensuring reliable characterization of the superconducting ground state.

In our analysis, we assume an attractive electron-electron interaction in p WMs, leading to the emergence of superconductivity. Existence of such phonon mediated interaction is unknown at this moment since very few candidate materials have been proposed e.g. CeNiAsO [9], NiI₂ [17], Gd₃(Ru_{1- δ} Rh _{δ})₄Al₁₂ [18] etc. Nevertheless, there are systems with noncollinear magnetic moments, similar to p WMs, where the onset of superconductivity has been experimentally reported such as MnP [108], CrAs [96] etc. One can also induce superconductivity in p WMs by proximitizing to a conventional BCS superconductors such as NbSe₂. We have analyzed the superconducting pairing correlations originating from the intra-orbital components. Exploring the stability of our proposed phases in presence of inter-orbital pairing terms remains an outlook for our future work.

In conclusion, our work sheds light on the role of newly proposed unconventional p WMs in realizing the underlying superconducting phases highlighting the intriguing ones with practical applications. While our theoretical model simulations were performed in a square lattice, it would be interesting to investigate the same in the Kagome lattice as found for CeNiAsCo [18]. Given the SDE is supported by the finite-momentum superconductivity in static case, one can also study the mechanism and possibility of rectification effect in a superconducting diode via Floquet driving.

Methods

Topological invariant

The emergence of TSC phase in the BCS s -wave channel has been characterized by the winding number \mathcal{N}_x (\mathbb{Z} invariant) belonging to the BDI topological class of the ten-fold classification [101]. To compute the winding number, we first recast the BdG Hamiltonian $\mathcal{H}_{\text{BdG}}^{\text{BCS}}(\mathbf{k})$ of Eq. (10) into an anti-diagonal form by employing a unitary transformation as,

$$\tilde{\mathcal{H}}(\mathbf{k}) = \mathcal{U}_s^\dagger \mathcal{H}_{\text{BdG}}^{\text{BCS}}(\mathbf{k}) \mathcal{U}_s = \begin{pmatrix} 0 & q(\mathbf{k}) \\ q^\dagger(\mathbf{k}) & 0 \end{pmatrix} \quad (14)$$

where the unitary matrix, \mathcal{U}_s , diagonalizes the chiral symmetry operator, $\mathcal{S} = \pi_x \sigma_y \tau_x$, i.e., $\mathcal{U}_s^\dagger \mathcal{S} \mathcal{U}_s = \text{diag}(-1, -1, -1, -1, 1, 1, 1, 1)$. The 4×4 block $q(\mathbf{k})$ used

in Eq. (11) is given by,

$$q(\mathbf{k}) = \begin{pmatrix} \xi(\mathbf{k}) - \alpha(\mathbf{k}) & -i\Delta^c & J_{sd} & 0 \\ -i\Delta^c & \xi(\mathbf{k}) - \alpha(\mathbf{k}) & 0 & -J_{sd} \\ J_{sd} & 0 & \xi(\mathbf{k}) + \alpha(\mathbf{k}) & -i\Delta^c \\ 0 & -J_{sd} & -i\Delta^c & \xi(\mathbf{k}) + \alpha(\mathbf{k}) \end{pmatrix},$$

where, $\xi(\mathbf{k})$ and $\alpha(\mathbf{k})$ are as per the definitions given in the main text. Using this form of the $q(\mathbf{k})$ matrix, we numerically compute the winding number, \mathcal{N}_x , taking into account the self-consistently obtained superconducting order parameter.

Hamiltonians for finite size geometries.

To illustrate the appearance of MFEMs, we investigate the spectral properties of the BdG Hamiltonian considering both the ribbon and rectangular geometries. In the ribbon geometry, we choose a finite size system of length L_x along x -direction under open boundary conditions, while the system remains periodic along the y -direction, thus keeping k_y as a good quantum number. The corresponding Hamiltonian is obtained by performing an inverse Fourier transformation of the Nambu basis along x -direction as,

$$\Psi_{k_x, k_y} = \frac{1}{L_x} \sum_{x=1}^{L_x} e^{ik_x x} \Psi_{x, k_y}. \quad (16)$$

The mean-field BdG Hamiltonian in the BCS channel (see Eq. (10)) is given by,

$$H_{\text{BdG}} = \sum_{k_x, k_y} \Psi_{k_x, k_y}^\dagger [\xi(\mathbf{k})\pi_z + \alpha(\mathbf{k})\sigma_z + J_{sd}\pi_z\sigma_x\tau_z + \Delta^c\pi_y\sigma_y] \Psi_{k_x, k_y}, \quad (17)$$

We then replace Eq. (16) in Eq. (17) and after simplification we obtain the Hamiltonian for the ribbon geometry as,

$$H_{\text{BdG}} = \sum_{x=1}^{L_x} \sum_{k_y} \Psi_{x, k_y}^\dagger [(-2t \cos k_y - \mu)\pi_z + J_{sd}\pi_z\sigma_x\tau_z + \Delta^c\pi_y\sigma_y] \Psi_{x, k_y} + \Psi_{x, k_y}^\dagger \left[-t\pi_z + \frac{\alpha}{2i}\sigma_z\right] \Psi_{x+1, k_y} + \text{H.c.} \quad (18)$$

In case of the rectangular geometry, we consider a finite size system along both x - and y -directions with lengths L_x and L_y , respectively, under the open boundary condition. Then, we perform the inverse Fourier transformation of the Nambu basis along both x - and y -directions as,

$$\Psi_{k_x, k_y} = \frac{1}{L_x L_y} \sum_{x=1}^{L_x} \sum_{y=1}^{L_y} e^{ik_x x} e^{ik_y y} \Psi_{x, y}. \quad (19)$$

We again replace Eq. (19) in Eq. (17), and obtain the Hamiltonian for the rectangular geometry as,

$$H_{\text{BdG}} = \sum_{x=1}^{L_x} \sum_{y=1}^{L_y} \Psi_{x, y}^\dagger [-\mu\pi_z + J_{sd}\pi_z\sigma_x\tau_z + \Delta^c\pi_y\sigma_y] \Psi_{x, y} + \Psi_{x, y}^\dagger \left[-t\pi_z + \frac{\alpha}{2i}\sigma_z\right] \Psi_{x+1, y} + \Psi_{x, y}^\dagger [-t\pi_z] \Psi_{x, y+1} + \text{H.c.}, \quad (20)$$

We employ the Hamiltonians described in Eqs. (18) and (20) to investigate the emergence of MFEMs and their edge localization in the TSC phase.

Data Availability

The datasets generated and analyzed during the current study are available from the authors upon reasonable request.

Code Availability

The codes and data generated during this study are available from the authors upon request.

Acknowledgements

A.P. acknowledges Ganpathy Murthy, Mathias S. Scheurer, Arnob Kumar Ghosh, Suman Jyoti De, and Moonsum Pervez for stimulating discussions. A.P. and A.S. acknowledge the SAMKHYA: High-Performance Computing facility provided by the Institute of Physics, Bhubaneswar and the two Workstations provided by the Institute of Physics, Bhubaneswar from the DAE APEX Project for numerical computations. P.D. acknowledges the Department of Space (DoS), India for all support at Physical Research Laboratory (PRL).

Authors contributions

P.D. and A.S. jointly conceived the idea and supervised the project. A.P. performed all calculations and prepared the manuscript with input from P.D. and A.S. All authors contributed to the science discussions and manuscript preparation.

* paramita@prl.res.in

† arijit@iopb.res.in

- [1] L. Šmejkal, J. Sinova, and T. Jungwirth, “Beyond Conventional Ferromagnetism and Antiferromagnetism: A Phase with Nonrelativistic Spin and Crystal Rotation Symmetry,” *Phys. Rev. X* **12**, 031042 (2022).
- [2] L. Šmejkal, J. Sinova, and T. Jungwirth, “Emerging Research Landscape of Altermagnetism,” *Phys. Rev. X* **12**, 040501 (2022).
- [3] S. Bhowal and N. A. Spaldin, “Ferroically Ordered Magnetic Octupoles in d -Wave Altermagnets,” *Phys. Rev. X* **14**, 011019 (2024).
- [4] I. I. Mazin, “Altermagnetism in MnTe : Origin, predicted manifestations, and routes to detwinning,” *Phys. Rev. B* **107**, L100418 (2023).

- [5] S. Lee, S. Lee, S. Jung, J. Jung, D. Kim, Y. Lee, B. Seok, J. Kim, B. G. Park, L. Šmejkal, C.-J. Kang, and C. Kim, “Broken Kramers Degeneracy in Altermagnetic MnTe,” *Phys. Rev. Lett.* **132**, 036702 (2024).
- [6] S. Biswas, P. Dutta, *et al.*, “Altermagnetic phases and phase transitions in Lieb-5 Hubbard model,” arXiv preprint arXiv:2601.14200 (2026).
- [7] A. B. Hellenes, T. Jungwirth, R. Jaeschke-Ubiergo, A. Chakraborty, J. Sinova, and L. Šmejkal, “P-wave magnets,” (2024), arXiv:2309.01607 [cond-mat.mes-hall].
- [8] B. Brekke, P. Sukhachov, H. G. Giil, A. Brataas, and J. Linder, “Minimal Models and Transport Properties of Unconventional p-Wave Magnets,” *Phys. Rev. Lett.* **133**, 236703 (2024).
- [9] A. Chakraborty, A. Birk Hellenes, R. Jaeschke-Ubiergo, T. Jungwirth, L. Šmejkal, and J. Sinova, “Highly efficient non-relativistic Edelstein effect in nodal p-wave magnets,” *Nature Communications* **16**, 7270 (2025).
- [10] D. McNally, “P-wave magnetism in a metal,” *Nature Materials* **25**, 16 (2026).
- [11] P. Sukhachov, H. G. Giil, B. Brekke, and J. Linder, “Coexistence of p-wave magnetism and superconductivity,” *Phys. Rev. B* **111**, L220403 (2025).
- [12] Y. Fukaya, K. Maeda, K. Yada, J. Cayao, Y. Tanaka, and B. Lu, “Josephson effect and odd-frequency pairing in superconducting junctions with unconventional magnets,” *Phys. Rev. B* **111**, 064502 (2025).
- [13] M. Ezawa, “Purely electrical detection of the spin-splitting vector in p-wave magnets based on linear and nonlinear conductivities,” *Phys. Rev. B* **112**, 125412 (2025).
- [14] M. Ezawa, “Out-of-plane Edelstein effects: Electric field induced magnetization in p-wave magnets,” *Phys. Rev. B* **111**, L161301 (2025).
- [15] Y. Nagae, L. Katayama, and S. Ikegaya, “Flat-band zero-energy states and anomalous proximity effects in p-wave magnet–superconductor hybrid systems,” *Phys. Rev. B* **111**, 174519 (2025).
- [16] T. Kokkeler, I. Tokatly, and F. S. Bergeret, “Quantum transport theory for unconventional magnets: Interplay of altermagnetism and p-wave magnetism with superconductivity,” *SciPost Phys.* **18**, 178 (2025).
- [17] Q. Song, S. Stavrić, P. Barone, A. Droghetti, D. S. Antonenko, J. W. F. Venderbos, C. A. Occhialini, B. Ilyas, E. Ergeçen, N. Gedik, S.-W. Cheong, R. M. Fernandes, S. Picozzi, and R. Comin, “Electrical switching of a p-wave magnet,” *Nature* **642**, 64 (2025).
- [18] R. Yamada, M. T. Birch, P. R. Baral, S. Okumura, R. Nakano, S. Gao, M. Ezawa, T. Nomoto, J. Masell, Y. Ishihara, K. K. Kolincio, I. Belopolski, H. Sagayama, H. Nakao, K. Ohishi, T. Ohhara, R. Kiyonagi, T. Nakajima, Y. Tokura, T.-h. Arima, Y. Motome, M. M. Hirschmann, and M. Hirschberger, “A metallic p-wave magnet with commensurate spin helix,” *Nature* **646**, 837 (2025).
- [19] M. Maple, “Interplay between superconductivity and magnetism,” *Physica B: Condensed Matter* **215**, 110 (1995), magnetism and Superconductivity.
- [20] M. Sgrist, “Introduction to unconventional superconductivity in non-centrosymmetric metals,” *AIP Conference Proceedings* **1162**, 55 (2009).
- [21] A. B. Karki, V. O. Garlea, R. Custelcean, S. Stadler, E. W. Plummer, and R. Jin, “Interplay between superconductivity and magnetism in Fe_{1-x}PdxTe,” *Proceedings of the National Academy of Sciences* **110**, 9283 (2013).
- [22] A. I. Buzdin, “Proximity effects in superconductor-ferromagnet heterostructures,” *Rev. Mod. Phys.* **77**, 935 (2005).
- [23] F. S. Bergeret, A. F. Volkov, and K. B. Efetov, “Odd triplet superconductivity and related phenomena in superconductor-ferromagnet structures,” *Rev. Mod. Phys.* **77**, 1321 (2005).
- [24] A. Y. Kitaev, “Unpaired Majorana fermions in quantum wires,” *Physics-Uspekhi* **44**, 131 (2001).
- [25] J. Alicea, “New directions in the pursuit of Majorana fermions in solid state systems,” *Reports on Progress in Physics* **75**, 076501 (2012).
- [26] J. Alicea, Y. Oreg, G. Refael, F. von Oppen, and M. P. A. Fisher, “Non-Abelian statistics and topological quantum information processing in 1D wire networks,” *Nature Physics* **7**, 412 (2011).
- [27] C. Beenakker, “Search for Majorana fermions in superconductors,” *Annu. Rev. Condens. Matter Phys.* **4**, 113 (2013).
- [28] N. F. Q. Yuan and L. Fu, “Topological metals and finite-momentum superconductors,” *Proceedings of the National Academy of Sciences* **118**, e2019063118 (2021).
- [29] J. J. Kinnunen, J. E. Baarsma, J.-P. Martikainen, and P. Törmä, “The Fulde–Ferrell–Larkin–Ovchinnikov state for ultracold fermions in lattice and harmonic potentials: a review,” *Reports on Progress in Physics* **81**, 046401 (2018).
- [30] S.-B. Zhang, L.-H. Hu, and T. Neupert, “Finite-momentum Cooper pairing in proximitized altermagnets,” *Nature Communications* **15**, 1801 (2024).
- [31] D. Chakraborty and A. M. Black-Schaffer, “Constraints on superconducting pairing in altermagnets,” *Phys. Rev. B* **112**, 014516 (2025).
- [32] D. Chakraborty and A. M. Black-Schaffer, “Perfect Superconducting Diode Effect in Altermagnets,” *Phys. Rev. Lett.* **135**, 026001 (2025).
- [33] S. A. A. Ghorashi, T. L. Hughes, and J. Cano, “Altermagnetic Routes to Majorana Modes in Zero Net Magnetization,” *Phys. Rev. Lett.* **133**, 106601 (2024).
- [34] Y.-X. Li, “Realizing tunable higher-order topological superconductors with altermagnets,” *Phys. Rev. B* **109**, 224502 (2024).
- [35] Y.-X. Li and C.-C. Liu, “Majorana corner modes and tunable patterns in an altermagnet heterostructure,” *Phys. Rev. B* **108**, 205410 (2023).
- [36] D. Zhu, Z.-Y. Zhuang, Z. Wu, and Z. Yan, “Topological superconductivity in two-dimensional altermagnetic metals,” *Phys. Rev. B* **108**, 184505 (2023).
- [37] H. Zhang, Ö. Gül, S. Conesa-Boj, M. P. Nowak, M. Wimmer, K. Zuo, V. Mourik, F. K. de Vries, J. van Veen, M. W. A. de Moor, J. D. S. Bommer, D. J. van Woerkom, D. Car, S. R. Plissard, E. P. Bakkers, M. Quintero-Pérez, M. C. Cassidy, S. Koelling, S. Goswami, K. Watanabe, T. Taniguchi, and L. P. Kouwenhoven, “Ballistic superconductivity in semiconductor nanowires,” *Nature Communications* **8**, 16025 (2017).
- [38] D. Mondal, A. Pal, A. Saha, and T. Nag, “Distinguishing between topological Majorana and trivial zero modes via transport and shot noise study in an altermagnet

- heterostructure,” *Phys. Rev. B* **111**, L121401 (2025).
- [39] A. Pal, D. Mondal, T. Nag, and A. Saha, “Josephson current signature of Floquet Majorana and topological accidental zero modes in altermagnet heterostructures,” *Phys. Rev. B* **112**, L201408 (2025).
- [40] O. Alam, A. Pal, P. Dutta, and A. Saha, “Proximity-induced superconductivity and emerging topological phases in altermagnet-based heterostructures,” arXiv:2510.26894 [cond-mat.supr-con].
- [41] K. Maeda, Y. Fukaya, K. Yada, B. Lu, Y. Tanaka, and J. Cayao, “Classification of pair symmetries in superconductors with unconventional magnetism,” *Phys. Rev. B* **111**, 144508 (2025).
- [42] P. Chatterjee and V. Juričić, “Interplay between altermagnetism and topological superconductivity on an unconventional superconducting platform,” *Phys. Rev. B* **112**, 054503 (2025).
- [43] S. S. Ruthvik and T. Nag, “Field-free diode effects in one-dimensional superconductor: a complex interplay between Fulde-Ferrell pairing and altermagnetism,” arXiv:2512.01415 [cond-mat.mes-hall].
- [44] R. M. Lutchyn, J. D. Sau, and S. Das Sarma, “Majorana Fermions and a Topological Phase Transition in Semiconductor-Superconductor Heterostructures,” *Phys. Rev. Lett.* **105**, 077001 (2010).
- [45] M. Leijnse and K. Flensberg, “Introduction to topological superconductivity and Majorana fermions,” *Semiconductor Science and Technology* **27**, 124003 (2012).
- [46] A. Das, Y. Ronen, Y. Most, Y. Oreg, M. Heiblum, and H. Shtrikman, “Zero-bias peaks and splitting in an Al-InAs nanowire topological superconductor as a signature of Majorana fermions,” *Nature Physics* **8**, 887 (2012).
- [47] Z.-Z. Li, F.-C. Zhang, and Q.-H. Wang, “Majorana modes in a topological insulator/s-wave superconductor heterostructure,” *Scientific Reports* **4**, 6363 (2014).
- [48] P. Fulde and R. A. Ferrell, “Superconductivity in a Strong Spin-Exchange Field,” *Phys. Rev.* **135**, A550 (1964).
- [49] A. I. Larkin and Y. N. Ovchinnikov, “Nonuniform state of superconductors,” *Zh. Eksp. Teor. Fiz.* **47**, 1136 (1964).
- [50] Z. Zhu, M. Papaj, X.-A. Nie, H.-K. Xu, Y.-S. Gu, X. Yang, D. Guan, S. Wang, Y. Li, C. Liu, J. Luo, Z.-A. Xu, H. Zheng, L. Fu, and J.-F. Jia, “Discovery of segmented Fermi surface induced by Cooper pair momentum,” *Science* **374**, 1381 (2021).
- [51] N. F. Q. Yuan and L. Fu, “Supercurrent diode effect and finite-momentum superconductors,” *Proceedings of the National Academy of Sciences* **119**, e2119548119 (2022).
- [52] A. Daido, Y. Ikeda, and Y. Yanase, “Intrinsic Superconducting Diode Effect,” *Phys. Rev. Lett.* **128**, 037001 (2022).
- [53] D. F. Agterberg, P. M. R. Brydon, and C. Timm, “Bogoliubov Fermi Surfaces in Superconductors with Broken Time-Reversal Symmetry,” *Phys. Rev. Lett.* **118**, 127001 (2017).
- [54] P. M. R. Brydon, D. F. Agterberg, H. Menke, and C. Timm, “Bogoliubov Fermi surfaces: General theory, magnetic order, and topology,” *Phys. Rev. B* **98**, 224509 (2018).
- [55] C. Setty, Y. Cao, A. Kreisel, S. Bhattacharyya, and P. J. Hirschfeld, “Bogoliubov Fermi surfaces in spin- $\frac{1}{2}$ systems: Model Hamiltonians and experimental consequences,” *Phys. Rev. B* **102**, 064504 (2020).
- [56] N. F. Q. Yuan and L. Fu, “Zeeman-induced gapless superconductivity with a partial Fermi surface,” *Phys. Rev. B* **97**, 115139 (2018).
- [57] C. Setty, S. Bhattacharyya, Y. Cao, A. Kreisel, and P. J. Hirschfeld, “Topological ultranodal pair states in iron-based superconductors,” *Nature Communications* **11**, 523 (2020).
- [58] C. J. Lapp, G. Börner, and C. Timm, “Experimental consequences of Bogoliubov Fermi surfaces,” *Phys. Rev. B* **101**, 024505 (2020).
- [59] S. Banerjee, S. Ikegaya, and A. P. Schnyder, “Anomalous Fano factor as a signature of Bogoliubov Fermi surfaces,” *Phys. Rev. Res.* **4**, L042049 (2022).
- [60] A. Pal, A. Saha, and P. Dutta, “Transport signatures of Bogoliubov Fermi surfaces in normal metal/time-reversal symmetry broken d-wave superconductor junctions,” *New Journal of Physics* **26**, 053027 (2024).
- [61] C. Timm, A. P. Schnyder, D. F. Agterberg, and P. M. R. Brydon, “Inflated nodes and surface states in superconducting half-Heusler compounds,” *Phys. Rev. B* **96**, 094526 (2017).
- [62] H. Oh and E.-G. Moon, “Instability of $j = \frac{3}{2}$ Bogoliubov Fermi surfaces,” *Phys. Rev. B* **102**, 020501 (2020).
- [63] C. Timm and A. Bhattacharyya, “Symmetry, nodal structure, and Bogoliubov Fermi surfaces for nonlocal pairing,” *Phys. Rev. B* **104**, 094529 (2021).
- [64] C. Timm, P. M. R. Brydon, and D. F. Agterberg, “Distortional weak-coupling instability of Bogoliubov Fermi surfaces,” *Phys. Rev. B* **103**, 024521 (2021).
- [65] P. Dutta, F. Parhizgar, and A. M. Black-Schaffer, “Superconductivity in spin-3/2 systems: Symmetry classification, odd-frequency pairs, and Bogoliubov Fermi surfaces,” *Phys. Rev. Res.* **3**, 033255 (2021).
- [66] H. Menke, C. Timm, and P. M. R. Brydon, “Bogoliubov Fermi surfaces stabilized by spin-orbit coupling,” *Phys. Rev. B* **100**, 224505 (2019).
- [67] Y. Cao, C. Setty, L. Fanfarillo, A. Kreisel, and P. J. Hirschfeld, “Microscopic origin of ultranodal superconducting states in spin- $\frac{1}{2}$ systems,” *Phys. Rev. B* **108**, 224506 (2023).
- [68] M. Wei, L. Xiang, F. Xu, L. Zhang, G. Tang, and J. Wang, “Gapless superconducting state and mirage gap in altermagnets,” *Phys. Rev. B* **109**, L201404 (2024).
- [69] S. S. Babkin, A. P. Higginbotham, and M. Serbyn, “Proximity-induced gapless superconductivity in two-dimensional Rashba semiconductor in magnetic field,” *SciPost Phys.* **16**, 115 (2024).
- [70] A. Pal, P. Dutta, and A. Saha, “Identifying Bogoliubov Fermi surfaces via thermoelectric response in a d-wave superconductor heterostructure,” *Phys. Rev. B* **110**, 245417 (2024).
- [71] D. Phan, J. Senior, A. Ghazaryan, M. Hatefipour, W. M. Strickland, J. Shabani, M. Serbyn, and A. P. Higginbotham, “Detecting Induced $p \pm ip$ Pairing at the Al-InAs Interface with a Quantum Microwave Circuit,” *Phys. Rev. Lett.* **128**, 107701 (2022).
- [72] M. Nadeem, M. S. Fuhrer, and X. Wang, “The superconducting diode effect,” *Nature Reviews Physics* **5**, 558 (2023).
- [73] K. Jiang and J. Hu, “Superconducting diode effects,” *Nature Physics* **18**, 1145 (2022).
- [74] F. Ando, Y. Miyasaka, T. Li, J. Ishizuka, T. Arakawa, Y. Shiota, T. Moriyama, Y. Yanase, and T. Ono, “Observation of superconducting diode effect,” *Nature* **584**,

- 373 (2020).
- [75] H. Wu, Y. Wang, Y. Xu, P. K. Sivakumar, C. Pasco, U. Filippozzi, S. S. P. Parkin, Y.-J. Zeng, T. McQueen, and M. N. Ali, “*The field-free Josephson diode in a van der Waals heterostructure*,” *Nature* **604**, 653 (2022).
- [76] J.-X. Lin, P. Siriviboon, H. D. Scammell, S. Liu, D. Rhodes, K. Watanabe, T. Taniguchi, J. Hone, M. S. Scheurer, and J. I. A. Li, “*Zero-field superconducting diode effect in small-twist-angle trilayer graphene*,” *Nature Physics* **18**, 1221 (2022).
- [77] B. Pal, A. Chakraborty, P. K. Sivakumar, M. Davydova, A. K. Gopi, A. K. Pandeya, J. A. Krieger, Y. Zhang, M. Date, S. Ju, N. Yuan, N. B. M. Schröter, L. Fu, and S. S. P. Parkin, “*Josephson diode effect from Cooper pair momentum in a topological semimetal*,” *Nature Physics* **18**, 1228 (2022).
- [78] P. Chatterjee and P. Dutta, “*Quasiparticles-mediated thermal diode effect in Weyl Josephson junctions*,” *New Journal of Physics* **26**, 073035 (2024).
- [79] S. Sachin, M. S. Scheurer, C. Schrade, and S. Manna, “*Altermagnetic Superconducting Diode Effect in Mn₃Pt/Nb Heterostructures*,” arXiv:2601.03366 [cond-mat.mes-hall].
- [80] S. Ilić and F. S. Bergeret, “*Theory of the Supercurrent Diode Effect in Rashba Superconductors with Arbitrary Disorder*,” *Phys. Rev. Lett.* **128**, 177001 (2022).
- [81] H. F. Legg, D. Loss, and J. Klinovaja, “*Superconducting diode effect due to magnetochiral anisotropy in topological insulators and Rashba nanowires*,” *Phys. Rev. B* **106**, 104501 (2022).
- [82] J. Hasan, D. Shaffer, M. Khodas, and A. Levchenko, “*Supercurrent diode effect in helical superconductors*,” *Phys. Rev. B* **110**, 024508 (2024).
- [83] S. Bhowmik and A. Saha, “*Topological Majorana zero modes and the superconducting diode effect driven by Fulde-Ferrell-Larkin-Ovchinnikov pairing in a helical Shiba chain*,” *Phys. Rev. B* **111**, L161402 (2025).
- [84] D. Samanta and S. K. Ghosh, “*Field-free Superconducting Diode Effect and Topological Fulde-Ferrell-Larkin-Ovchinnikov Superconductivity in Altermagnetic Shiba Chains*,” arXiv:2507.21446 [cond-mat.supr-con].
- [85] M. Davydova, S. Prembabu, and L. Fu, “*Universal Josephson diode effect*,” *Science Advances* **8**, eabo0309 (2022).
- [86] H. F. Legg, K. Laubscher, D. Loss, and J. Klinovaja, “*Parity-protected superconducting diode effect in topological Josephson junctions*,” *Phys. Rev. B* **108**, 214520 (2023).
- [87] D. Debnath and P. Dutta, “*Gate-tunable Josephson diode effect in Rashba spin-orbit coupled quantum dot junctions*,” *Phys. Rev. B* **109**, 174511 (2024).
- [88] D. Debnath and P. Dutta, “*Field-free Josephson diode effect in interacting chiral quantum dot junctions*,” *Journal of Physics: Condensed Matter* **37**, 175301 (2025).
- [89] D. Debnath, A. Saha, and P. Dutta, “*Spin-polarization and diode effect in thermoelectric current through altermagnet-based superconductor heterostructures*,” arXiv:2509.12198 [cond-mat.supr-con].
- [90] S. Banerjee and M. S. Scheurer, “*Altermagnetic superconducting diode effect*,” *Phys. Rev. B* **110**, 024503 (2024).
- [91] A. Pal, D. Mondal, T. Nag, and A. Saha, “*Topological superconductivity and superconducting diode effect mediated via unconventional magnet and Ising spin-orbit coupling*,” arXiv:2512.01266 [cond-mat.mes-hall].
- [92] C. Schrade, S. Manna, and M. S. Scheurer, “*Altermagnetic superconducting diode effect from non-collinear compensated magnetism in Mn₃Pt*,” arXiv:2601.03348 [cond-mat.mes-hall].
- [93] L. Sharma, B. Ghimire, and M. Thakurathi, “*p-wave magnet driven field-free Josephson diode effect*,” arXiv:2602.16677 [cond-mat.supr-con].
- [94] S. Banerjee and M. S. Scheurer, “*Enhanced Superconducting Diode Effect due to Coexisting Phases*,” *Phys. Rev. Lett.* **132**, 046003 (2024).
- [95] S. Bhowmik, D. Samanta, A. K. Nandy, A. Saha, and S. K. Ghosh, “*Optimizing one dimensional superconducting diodes: interplay of Rashba spin-orbit coupling and magnetic fields*,” *Communications Physics* **8**, 260 (2025).
- [96] H. Kotegawa, S. Nakahara, H. Tou, and H. Sugawara, “*Superconductivity of 2.2 K under Pressure in Helimagnet CrAs*,” *Journal of the Physical Society of Japan* **83**, 093702 (2014).
- [97] C. W. J. Beenakker, “*Random-matrix theory of quantum transport*,” *Rev. Mod. Phys.* **69**, 731 (1997).
- [98] P. Coleman, *Introduction to Many-Body Physics* (Cambridge University Press, 2015).
- [99] A. M. Clogston, “*Upper Limit for the Critical Field in Hard Superconductors*,” *Phys. Rev. Lett.* **9**, 266 (1962).
- [100] B. S. Chandrasekhar, “*A note on the Maximum Critical Field of High-Field Superconductors*,” *Applied Physics Letters* **1**, 7 (1962).
- [101] C.-K. Chiu, J. C. Y. Teo, A. P. Schnyder, and S. Ryu, “*Classification of topological quantum matter with symmetries*,” *Rev. Mod. Phys.* **88**, 035005 (2016).
- [102] S. Ryu, A. P. Schnyder, A. Furusaki, and A. W. W. Ludwig, “*Topological insulators and superconductors: tenfold way and dimensional hierarchy*,” *New Journal of Physics* **12**, 065010 (2010).
- [103] W. A. Benalcazar and A. Cerjan, “*Chiral-Symmetric Higher-Order Topological Phases of Matter*,” *Phys. Rev. Lett.* **128**, 127601 (2022).
- [104] A. Pal and A. K. Ghosh, “*Multi-higher-order Dirac and nodal line semimetals*,” *Phys. Rev. B* **111**, 195429 (2025).
- [105] K. L. Zhang, P. Wang, and Z. Song, “*Majorana flat band edge modes of topological gapless phase in 2D Kitaev square lattice*,” *Scientific Reports* **9**, 4978 (2019).
- [106] S. Nakosai, Y. Tanaka, and N. Nagaosa, “*Two-dimensional p-wave superconducting states with magnetic moments on a conventional s-wave superconductor*,” *Phys. Rev. B* **88**, 180503 (2013).
- [107] P. Chatterjee, S. Banik, S. Bera, A. K. Ghosh, S. Pradhan, A. Saha, and A. K. Nandy, “*Topological superconductivity by engineering noncollinear magnetism in magnet/superconductor heterostructures: A realistic prescription for the two-dimensional Kitaev model*,” *Phys. Rev. B* **109**, L121301 (2024).
- [108] J.-G. Cheng, K. Matsubayashi, W. Wu, J. P. Sun, F. K. Lin, J. L. Luo, and Y. Uwatoko, “*Pressure Induced Superconductivity on the border of Magnetic Order in MnP*,” *Phys. Rev. Lett.* **114**, 117001 (2015).

Supplementary Material for “Emergent superconducting phases in unconventional p -wave magnets: Topological superconductivity, Bogoliubov Fermi surfaces and superconducting diode effect”

Amartya Pal ^{1,2}, Paramita Dutta ³ and Arijit Saha ^{1,2}

¹*Institute of Physics, Sachivalaya Marg, Bhubaneswar-751005, India*

²*Homi Bhabha National Institute, Training School Complex, Anushakti Nagar, Mumbai 400094, India*

³*Theoretical Physics Division, Physical Research Laboratory, Navrangpura, Ahmedabad-380009, India*

CONTENTS

References	9
Transition from gapped to gapless superconducting phase driven by finite-momentum Cooper pairs	i
Behavior of superconducting order parameter	ii

TRANSITION FROM GAPPED TO GAPLESS SUPERCONDUCTING PHASE DRIVEN BY FINITE-MOMENTUM COOPER PAIRS

In the main text, we have proposed that the finite-momentum Cooper pairs drive the system from a gapped to a gapless superconducting phase with both Fulde-Ferrel (FF) and Larkin–Ovchinnikov (LO) pairings. These gapless FF and LO pairing states host the unique Bogoliubov Fermi surfaces (BFSs) as zero-energy excitations. In this section, we further provide some additional results to support our findings of the main text.

We illustrate the behavior of the bulk superconducting gap with the variation of the external Zeeman field in Fig. 6. Notably, we consider the mean-field order parameter obtained self-consistently by minimizing the condensation energy density. The mean-field Bogoliubov-de Gennes (BdG) Hamiltonian (Eq. (9) of the main text) in the finite momentum pairing channel is given by,

$$\mathcal{H}_{\text{BdG}}(\mathbf{k}, \mathbf{q}^c) = \begin{bmatrix} \mathcal{H}_N(\mathbf{k} + \frac{\mathbf{q}^c}{2}) & -i\sigma_y \Delta^c \\ i\sigma_y \Delta^c & -\mathcal{H}_N^T(-\mathbf{k} + \frac{\mathbf{q}^c}{2}) \end{bmatrix}, \quad (\text{S1})$$

which corresponds to the ground state characterized by (q_x^c, q_y^c, Δ^c) and thus it depends on the parameters of the

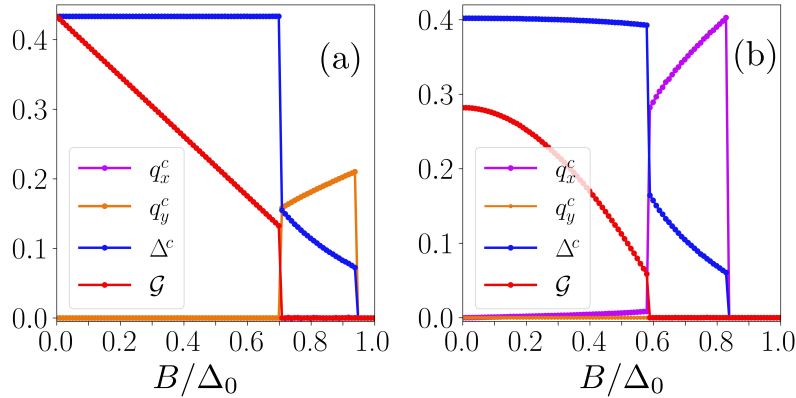


FIG. 6. Variation of superconducting order parameters, (q_x^c, q_y^c, Δ^c) and bulk BdG gap, \mathcal{G} are shown as a function of the external Zeeman field, B/Δ_0 in the LO (panel (a)) and FF pairing channels (panel (b)). We set $J_{sd}/\Delta_0 = 0$ (panel (a)) and $J_{sd}/\Delta_0 = 0.6$ (panel (b)). Other model parameters are chosen as $(\alpha, \mu, t) = (t, -2t, t)$.

Hamiltonian.

We first diagonalize the above Hamiltonian to obtain the energy eigenvalues, $\mathcal{E}(\mathbf{k})$, for each momentum point $\mathbf{k} = \{k_x, k_y\}$. Then, we compute the bulk gap as $\mathcal{G} = 2 \min_{\mathbf{k}} |\mathcal{E}(\mathbf{k})|$. We then depict the variation of \mathcal{G} as well as (q_x^c, q_y^c, Δ^c) as a function of the Zeeman field B/Δ_0 in the LO pairing channel (see Fig. 6(a)) and FF pairing channel

(see Fig. 6(b)). In the LO phase, we observe that the bulk gap of the BdG eigenvalue spectrum becomes gapless when $q_y^c \neq 0$ but $q_x^c = 0$. Remarkably, both Δ^c and q_y^c exhibits discontinuous behaviours when the system enters into the gapless phase. The value of the Δ^c is also reduced in this gapless phase. On the other hand, in the FF phase, the system initially remains gapped even the Cooper pairs acquire a small but finite momentum with $q_x^c \neq 0$ but $q_y^c = 0$. Then, the system becomes gapless associated with a discontinuous change in Δ^c and q_x^c only after a certain strength of B/Δ_0 . The amplitude of q_x^c also grows further in the gapless phase. This behavior is consistent with the behavior observed in the LO and FF pairing channels supporting our discussions in the main text.

BEHAVIOR OF SUPERCONDUCTING ORDER PARAMETER

In the main text, we have illustrated the behavior of the superconducting diode efficiency η in the FF pairing channel by varying the external Zeeman field for various choices of μ and J_{sd} (see Figs. 5(c-d) in the main text). For the sake of completeness and understanding, here we depict the variation of the mean-field superconducting order parameter Δ^c and also q_x^c for the same set of model parameters.

In Figs. 7(a) and (c), we depict the variation Δ^c and q_x^c , respectively as a function of the external Zeeman field, for three choices of chemical potential μ and $J_{sd} \neq 0$, $\alpha \neq 0$, while, the variation of Δ^c and q_x^c are shown for three choices of the exchange strength J_{sd} considering $\mu \neq 0$ and $\alpha \neq 0$ in Figs. 7(b) and (d) respectively. The behavior of Δ^c remains consistent and qualitatively similar for different values of the chemical potential before it becomes zero after the critical magnetic field as presented in Fig. 7(a). These phenomena remain qualitatively similar irrespective of the exact values of exchange coupling as shown in Fig. 7(b). From Figs. 7(c) and (d), we observe that the Cooper pair momentum, q_x^c , initially increases linearly with the Zeeman field but it changes discontinuously when the system enters into the gapless phase supporting our discussions in Sec. . As a consequence, the diode efficiency decreases significantly in the gapless FF phase compared to the gapped FF superconducting phase as discussed in the main text (see Figs. 5(c-d)). We also note that the maximum diode efficiency appears close to the point where the bulk becomes gapless. These behaviors are fully consistent with our analysis described in the main text.

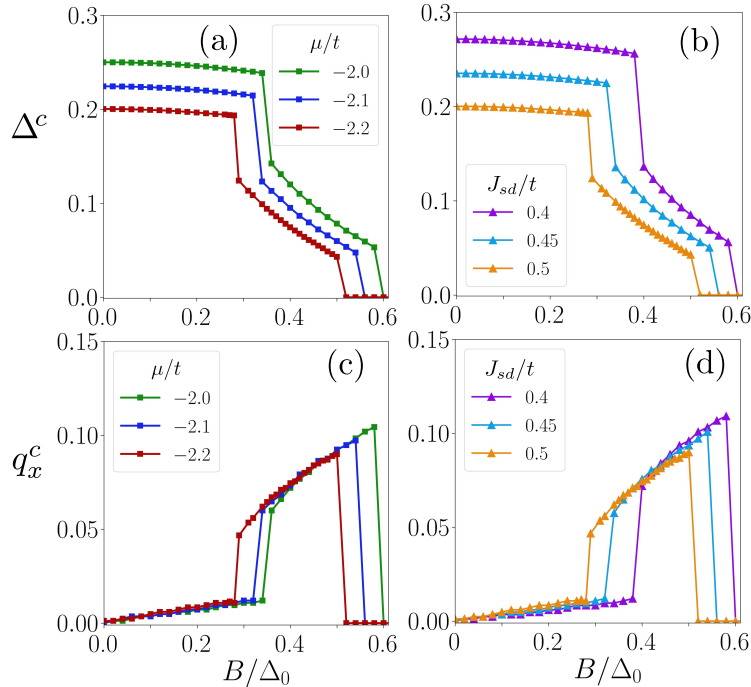


FIG. 7. Variation of Δ^c [(a)-(b)] and q_x^c [(c)-(d)] are displayed as functions of Zeeman field B/Δ_0 for various choices of the model parameters. In panels (a), (c), we set $(J_{sd}, \alpha) = (0.5t, t)$ whereas in panels (b), (d) we choose $(\mu, \alpha) = (-2.2t, t)$.